Measured electrical charge of SiO2 in polar and nonpolar media

Kokot, Gašper ; Bespalova, Maria I ; Krishnan, Madhavi

Abstract: We present measurements of the net electrical surface charge of silicon dioxide (SiO2) in contact with solvents of dielectric constants between 5 and 80. Our experimental approach relies on observing the thermal motion of single silica particles confined in an electrostatic fluidic trap created by SiO2 surfaces. We compare the experimentally measured functional form of the trapping potential with that from free energy calculations and thereby determine the net surface charge in the system. Our findings clearly demonstrate that contrary to popular perception, even in the absence of surfactants, the net electrical charge of ionizable surfaces in contact with apolar solvents can be large enough to lead to significant repulsive forces. A charge regulation model for SiO2 surfaces with a single tunable parameter explains our measurements. This model may find general applicability in estimating the net charge of ionizable surfaces, given system parameters such as the dissociation or association constants of the ionizable groups and the pH, ionic strength, and dielectric constant of the solvent phase.

DOI: https://doi.org/10.1063/1.4967401

Measured electrical charge of SiO_2 in polar and nonpolar media

G. Kokot, M. I. Bespalova, and M. Krishnan

Citation: J. Chem. Phys. **145**, 194701 (2016); doi: 10.1063/1.4967401
View online: http://dx.doi.org/10.1063/1.4967401
View Table of Contents: http://aip.scitation.org/toc/jcp/145/19
Published by the American Institute of Physics

Measured electrical charge of SiO_2 in polar and nonpolar media

G. Kokot,[1,a)] M. I. Bespalova,[1,a)] and M. Krishnan[1,2,b)]
[1]*Department of Chemistry, University of Zurich, Winterthurerstrasse 190, CH 8057 Zurich, Switzerland*
[2]*Department of Physics, University of Zurich, Winterthurerstrasse 190, CH 8057 Zurich, Switzerland*

(Received 1 September 2016; accepted 27 October 2016; published online 15 November 2016)

We present measurements of the net electrical surface charge of silicon dioxide (SiO_2) in contact with solvents of dielectric constants between 5 and 80. Our experimental approach relies on observing the thermal motion of single silica particles confined in an electrostatic fluidic trap created by SiO_2 surfaces. We compare the experimentally measured functional form of the trapping potential with that from free energy calculations and thereby determine the net surface charge in the system. Our findings clearly demonstrate that contrary to popular perception, even in the absence of surfactants, the net electrical charge of ionizable surfaces in contact with apolar solvents can be large enough to lead to significant repulsive forces. A charge regulation model for SiO_2 surfaces with a single tunable parameter explains our measurements. This model may find general applicability in estimating the net charge of ionizable surfaces, given system parameters such as the dissociation or association constants of the ionizable groups and the pH, ionic strength, and dielectric constant of the solvent phase. *Published by AIP Publishing.* [http://dx.doi.org/10.1063/1.4967401]

I. INTRODUCTION

An ionizable chemical group in a solvent dissociates to yield a charged group and a free counterion; for many inorganic oxides in solution, the counterion is a proton. A surface carrying a large number of ionizable groups denoted by a density Γ thus acquires a net charge density, σ in contact with a polar medium, with the balance of electrostatics and entropy determining the magnitude of this net surface charge. Charged colloidal particles and surfaces in solution interact via a screened electrostatic interaction, described by Derjaguin-Landau-Verwey-Overbeek (DLVO) theory[1] and considered largely well understood. In the aqueous phase, mutual repulsions between particles can be strong enough to stabilize dense suspensions of colloidal particles against aggregation, and indeed the principle of charge stabilization is ubiquitous in nature and in industrial formulations.

In low dielectric media, however, the electrostatic self energy of an ion, which depends inversely on the medium's dielectric constant, ε_s, is high, rendering the formation of free ions highly statistically unlikely. Thus, while matter can be expected to be strongly charged in water ($\varepsilon_s \sim 80$), an ionizable surface should carry much less charge in a nonpolar medium with $\varepsilon_s \sim 5$. Although electrostatic interactions in apolar media are indeed weak relative to the aqueous phase,[2–7] the repulsion is often regarded as negligible[8,9] mainly on the basis of solvation energy arguments. Generally efforts are invested in enhancing repulsions in apolar media by the addition of micelle-forming surfactants that stabilize potential-determining ions[2–7,9] or by chemical modification of the surface.[3,4,9] Electrostatic interactions in nonpolar media have been exploited in model systems for atomic crystals[10,11] in chemical formulations[12] and technological applications such as electronic ink.[13,14] Knowledge of the surface charge of ionizable matter suspended in weakly polar or nonpolar media is important not only from a charge stabilization perspective but also from the more fundamental point of view of understanding, quantifying, and delineating the various contributions to the total interaction potential between colloidal particles or surfaces in various intervening media.

Several experimental techniques have been used to estimate the charge of colloidal particles in nonpolar media. In the electrokinetic approach, which is possibly the most widespread, the mobility of a particle an electric field is used as a measure of the electrical potential at the particle surface, namely, the zeta potential. The zeta potential in turn can be related to the electrical charge carried by the particle. The approach has been implemented in various forms on free particles in a DC electric field[4,15,16] or using an alternating field in combination with the particle-position control implemented optically[2,17] or piezoelectrically.[18] Fast detection and long observation times have further enabled the measurement of temporal fluctuations in electrical charge on very weakly charged optically trapped particles in a nonpolar solvent.[17] Techniques that probe the charge of particles by measuring their mutual interactions in an ensemble at equilibrium, in the absence of fields, have also been successfully implemented in nonpolar media containing surfactants.[3,19]

In this study we perform direct measurements of the equilibrium repulsive electrostatic potential of silica surfaces interacting across pure aqueous and organic solvents, namely, water (H_2O, $\varepsilon_s = 78.3$), acetonitrile (MeCN, $\varepsilon_s = 36.64$), ethanol (EtOH, $\varepsilon_s = 24.3$), and bromobenzene (BBr, $\varepsilon_s = 5.4$), with no added surfactants. Our approach to the problem of measuring a particle-surface interaction potential exploits the electrostatic fluidic trap for nano- or micron-scale matter in solution.[20–23] Briefly, the trap relies on the equilibrium thermodynamic

a)G. Kokot and M. I. Bespalova contributed equally to this work.
b)Electronic mail: madhavi.krishnan@uzh.ch

repulsion experienced by a particle confined in a fluid-filled micrometer-scale gap between the like-charged confining parallel plates. Micron-scale structuring of one of the slit surfaces leads to a modulation of the local electrostatic potential, creating a deep thermodynamic potential well for a like-charged entity (Fig. 1). We have previously demonstrated that in conjunction with a straightforward calculation of the trapping free energy, a direct optical measurement of the spatial sampling behavior of a single trapped particle can be used to measure its electrical charge with good precision.[21,23] In the present work, the walls of the slit and the particle are composed of SiO_2. Thus the theoretical model for the electrostatic free energy involves a single unknown parameter, namely, the regulated charge density, σ of the SiO_2 surfaces (slit and particle). Comparing the experimentally measured trapping potential for a single SiO_2 particle with a calculation of the spatial electrostatic interaction free energy where σ is a tunable parameter yields the net charge density of the SiO_2 surfaces in the system. Note that the entropic contribution to the total trap free energy arising from spatial fluctuations of the particle in z is estimated to be small (1%-10%) and therefore neglected in this work. Not only is the modeling of such a measurement more straightforward than, for example, the electrokinetic approach, but also in contrast our method probes the electrostatic interaction at equilibrium, at the single particle level, does not require calibration, and can be ubiquitously applied to particles and solvents of any polarity and composition.

In our measurements we encounter substantial repulsive electrostatic forces between silica surfaces even in a weakly polar solvent such as bromobenzene which was recently used as the intervening medium in an experiment to demonstrate the long range repulsive Casimir force between a gold and the silica surface.[8] Our measurements further permit us to estimate well the charge density of SiO_2 in contact with media of various polarities. Finally we apply a theoretical model that was originally proposed to describe the charge of SiO_2 and glass surfaces in water[24] to our measurements in various solvents. We find that the model captures our measurements of SiO_2 over the entire range of ε_s with the use of a single tunable parameter that contains the pH of the solvent and pK_a, the acid dissociation constant of the SiOH group in the solvent of interest. The results suggest that the model may be generally applied to estimate the electrostatic contribution to force measurements involving ionizable surfaces in the fluid phase.

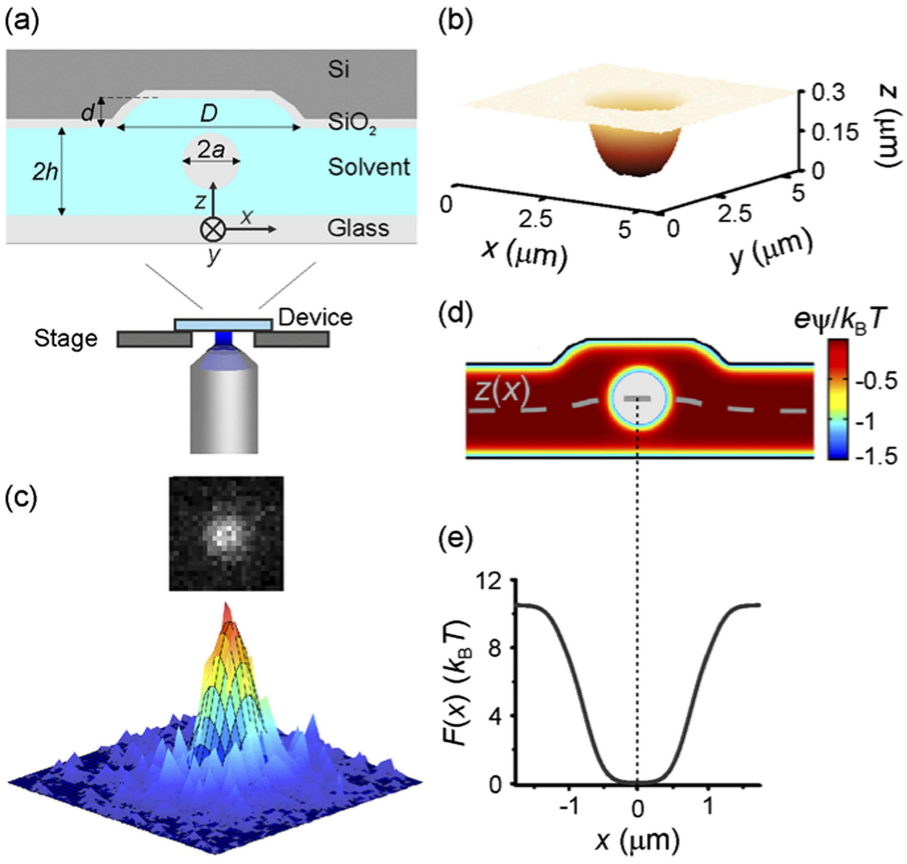

FIG. 1. (a) Schematic illustration of a single negatively charged SiO_2 microsphere of radius a, confined in an electrostatic fluidic trap, imaged using fluorescence microscopy. The cross-sectional view of a single trapping microstructure or pocket displays the relevant geometric parameters, namely, channel depth, $2h$; pocket depth, d; and pocket diameter, D. (b) 3D atomic force microscopy (AFM) image of pocket topography where the color scale spans a height range of 300 nm. (c) Typical fluorescence microscopy image of a single trapped particle (top), where the spatial intensity distribution (colormap, bottom) is fitted with an elliptical 2D Gaussian function (black contours). (d) Spatial electrostatic potential distribution, ψ around a particle in EtOH in a trapping microstructure (D = 2126 nm, $2h$ = 1139 nm, d = 308 nm, a = 325 nm). The dashed curve denotes the contour of minimum axial (z) electrostatic energy of the spherical particle as a function of lateral position, x. (e) Calculated spatial electrostatic free energy profile, $F(x)$ for parameter values in (d) for a particle surface charge density, $\sigma = -0.73 \times 10^{-3}$ e/nm^2.

II. EXPERIMENTAL METHODS

A. Electrostatic fluidic trap fabrication and characterization

The electrostatic fluidic trap devices were fabricated using a combination of photolithography and reactive-ion etching of Si substrates (for experiments in EtOH, MeCN, and H_2O) or wet-etching of glass substrates (for BBr), similar to previous work.[20] For measurements in EtOH, MeCN, and H_2O, the surface microstructures defining the trap locations were generally 300 nm deep and 2-2.2 μm in diameter, while the slit heights, $2h$, were in the range of 950-1150 nm. Surface features etched into Si substrate were coated with ~60 nm SiO_2. For experiments in BBr, however, the large Debye lengths involved (~400 nm) necessitated larger surface features with diameters, D, in the range 3.7-4.1 μm, depth, d ~ 1 μm, and slit height, $2h$ ~ 4 μm. Therefore for BBr experiments alone, the surface indentations were wet-etched into the glass substrate using HF as previously described.[20] Surface-microstructured fluidic slits were thus created by a glass surface on one side and a silica surface on the other. The trapping microstructures were characterized by scanning electron microscopy (SEM), profilometry, and atomic force microscopy (AFM); the various geometric parameters of interest such as slit height, pocket diameter, and depth are illustrated in Fig. 1.

B. Solvent conductivity and salt concentration

We performed single particle trapping experiments in bromobenzene, ethanol, acetonitrile (all >99% purity, Sigma Aldrich), and water. Water content of the pure solvents were <1%, <0.1%, and <0.005% for BBr, EtOH, and MeCN, respectively. Solvent conductivities and pH were measured using inoLab Cond 7110 (Xylem Analytics) and LAQUA Twin (Horiba Scientific) conductivity meters, and an Orion Star A215 (ThermoFisher Scientific) pH meter. For experiments in BBr we added tetrabutylammonium chloride (TBAC) salt at a nominal concentration of 8 M. Conductivity measurements however revealed that the fractional dissolution of added salt was only 0.5%, which is in fact in good agreement with previously reported results on ion association constants of large salt ions in solvents of low polarity[25] (see the supplementary material). The final dissolved concentration of ~0.04 M corresponds to a Debye screening length, $\kappa^{-1} = \sqrt{\frac{\varepsilon_s \varepsilon_0 k_B T}{2 N_A c e^2}} = 388$ nm. Here ε_s is the relative permittivity of the solvent, ε_0 is the permittivity of vacuum, N_A is the Avogadro number, c is the concentration of monovalent salt in moles/L, and e is the elementary charge. Due to the extremely low solubility of ions in BBr, we assume that the bulk solvent conductivity value prior to the experiment does indeed accurately reflect the salt concentration during the measurement. For measurements in MeCN and EtOH, our inability to measure low conductivities in the small fluid volumes of the device reservoir necessitated the treatment of c as a fitting parameter in the comparison of the measurements with the calculation. Measurements in H_2O were performed in 1 mM Tris Buffer, pH 8.7, and under an argon atmosphere, necessitated by the requirement of a stable pH, and the fact that the SiO_2 microspheres (diameter 650 ± 30 nm, Corpuscular, Inc.) were supplied in 1 M NaOH. For these experiments, pH and conductivity of the inlet and outlet reservoirs were measured at the end of each experiment using a microconductivity meter. All measured conductivities were converted to concentrations of monovalent salt using standard curves generated by a series of measurements at known salt concentrations (see the supplementary material).

Zeta potential of the silica microspheres were measured in EtOH, MeCN, and H_2O using laser doppler microelectrophoresis (Malvern, Zetasizer Nano ZS90) (Table II).

C. Single particle trapping, spatial potential profile measurements, and net surface charge determination

The fluorescently labeled silica particles were purified by repeated rounds (typically 5) of centrifugation and resuspension in the solvent of interest. The particles were initially loaded into the microslits by capillary flow. After a few minutes, the flow was arrested by loading both inlet and outlet reservoirs with the particle suspension. The device was sealed to prevent evaporation of the solvent during the experiment and allowed to equilibrate for 10 min before commencing with optical measurements. The dynamics of single trapped particles were recorded on time scales of several minutes using a home-built wide-field fluorescence microscopy setup and an electron-multiplying charge-coupled device (EMCCD) camera (Luca, Andor, Inc.). Images were acquired using exposure times of 10 ms, much smaller than the shortest estimated position relaxation time (~0.45 s) of the particle in the potential well.[26] Scatter plots of particle position were generated by fitting a 2D Gaussian function to the intensity profile in each image, as previously described[21] (Figs. 1(c) and 2(c)). Particle positions were thus determined with an average precision of less than 30 nm and then used to generate a radial probability density function, $P(r)$, and the corresponding experimentally measured trapping potential, $F(r) = -k_B T \ln \frac{P(r)}{P_{max}(r)}$ (Figs. 2(b), 2(d), and 3). Measured $P(r)$ for a given trapped particle were verified to be invariant for variable exposure times in the range 6-20 ms, ensuring that there were no exposure-time induced artifacts in the shape of the measured potential.[27] In order to relate the measured potential profiles, $F(r)$ to a net surface charge density in the system, calculations of the position dependent electrostatic free energy were carried out in COMSOL Multiphysics using constant charge boundary conditions as previously described.[22,28] Briefly, we numerically solved the non-linear Poisson-Boltzmann (PB) equation in the geometry shown in Fig. 1(d) and evaluated the electrostatic free energy as a function of particle position. The inputs to the calculation were the geometric parameters for the trapping microstructure, average particle diameter, and the dielectric constant of the solvent. For BBr and H_2O, the measured salt concentration, c of the solvent served as an input parameter, while for EtOH and MeCN, c was a free fitting parameter. Thus σ, and where applicable, c, was varied in the calculation and the best-fit theoretically predicted potentials were determined for each single particle data set. Figures 2 and 3 present experimentally measured confining potentials and the associated

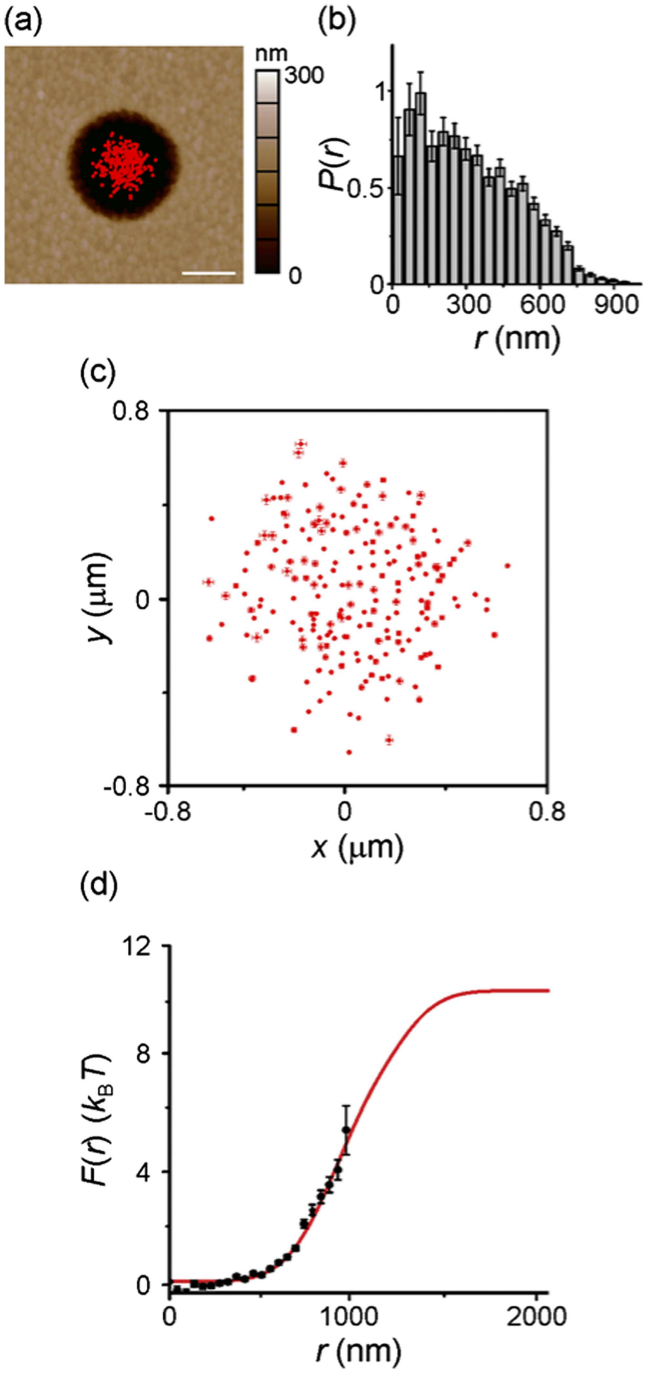

FIG. 2. Measurement of SiO_2 effective surface charge in ethanol. (a) Measured in-plane (x-y) trajectory of a single trapped particle superimposed on the AFM topographic image of the pocket. Each red symbol represents one detected position of the particle. (b) Histogram of the radial probability density, $P(r)$ for the data shown in (a). The displayed distribution was rescaled so that $P_{max}(r) = 1$. (c) The same scatter data as presented in (a) with error bars denoting precisions of localization. (d) Local electrostatic free energy, $F(r)$ (symbols) derived from the experimentally measured $P(r)$ presented in (b), and superimposed on the best-fit calculated potential profile (red line).

best-fit theoretically calculated free energy profiles for the representative single particles in all solvents. The resulting values of σ and κ^{-1} for each solvent together with other relevant system parameters are presented in Table I. We find that σ varies by over 2 orders of magnitude over the range of ε_s tested, with the uncertainty in particle size the dominant contribution to the measurement error (see below).

III. RESULTS AND DISCUSSION

In order to make controlled comparisons over a wide range of solvent polarities, we used the same probe particle sample in all measurements. Furthermore, since we expected a very low surface charge density for experiments in low-polarity solvents, we used a rather large particle size (radius, $a = 325 \pm 15$ nm) compared to our previous work in order to ensure a substantial trap depth of $\sim 10\ k_B T$. By doing so, however, it turned out impossible to achieve uniformly good measurement precision over the 4 order of magnitude range of experimental salt concentrations, necessitated by the range of solvent polarities examined. In water, for example, where κ^{-1} (~20 nm) $\ll a$ (~325 nm), the interaction between the particle and the slit walls, which determines the depth of the trap, resembles a parallel-plate interaction which in turn is exponentially sensitive to κa.[22] The dispersion in particle size thus implies large uncertainties in the value of the measured surface charge density. This uncertainty is further compounded by the non-linearity of the PB equation at the high net surface charge densities necessitated by the high pH ~9 under which the measurement had to be performed. As a result in this work, we are unable to place more than a lower bound on the net charge density of SiO_2 surfaces in water. The EtOH, MeCN, and BBr measurements on the other hand involve smaller values of κa and therefore do not display the same sensitivity of measured surface charge to particle size. The larger Debye lengths in these solvents also yield large well depths even though the net surface charge of the surfaces is relatively low (Table I). The experimental conditions were thus conducive to achieving a reasonable measurement precision of 15%-20% in these solvents.

Furthermore, despite the fact that it was not possible to reliably measure the true conductivity of the microliter solvent reservoirs in the experiments with non-aqueous solvents, the functional form of the measured trapping potential permitted independent determination of the effective screening length in the system as a fit parameter in the EtOH and MeCN measurements. We point out that in BBr, the large Debye lengths that result from weak dissociation of added salt[10,29] resulted in harmonic potential wells for the microstructure geometry used (d ≈ 4 μm) (Fig. 3(c)). Leaving the screening length (salt concentration) as a fit parameter as we did for EtOH and MeCN, it was possible to clearly establish an upper bound on the concentration. However given the dimension of the trapping microstructure, d ≈ 4 μm in the present experiment, it was impossible to establish a lower bound on the concentration in a fitting procedure where the charge density of the system is unknown in addition. Although experiments and theory involving high ion concentrations in apolar media suggest that the formation of Bjerrum pairs can greatly inflate the Debye length,[30,31] at the low concentrations of added TBAC (~10^{-5}M) in our experiment, the measurement is well within the regime where the screening length should be correctly estimated by the conductivity-based measurement of free ions.[31] So for BBr we used the measured salt concentration

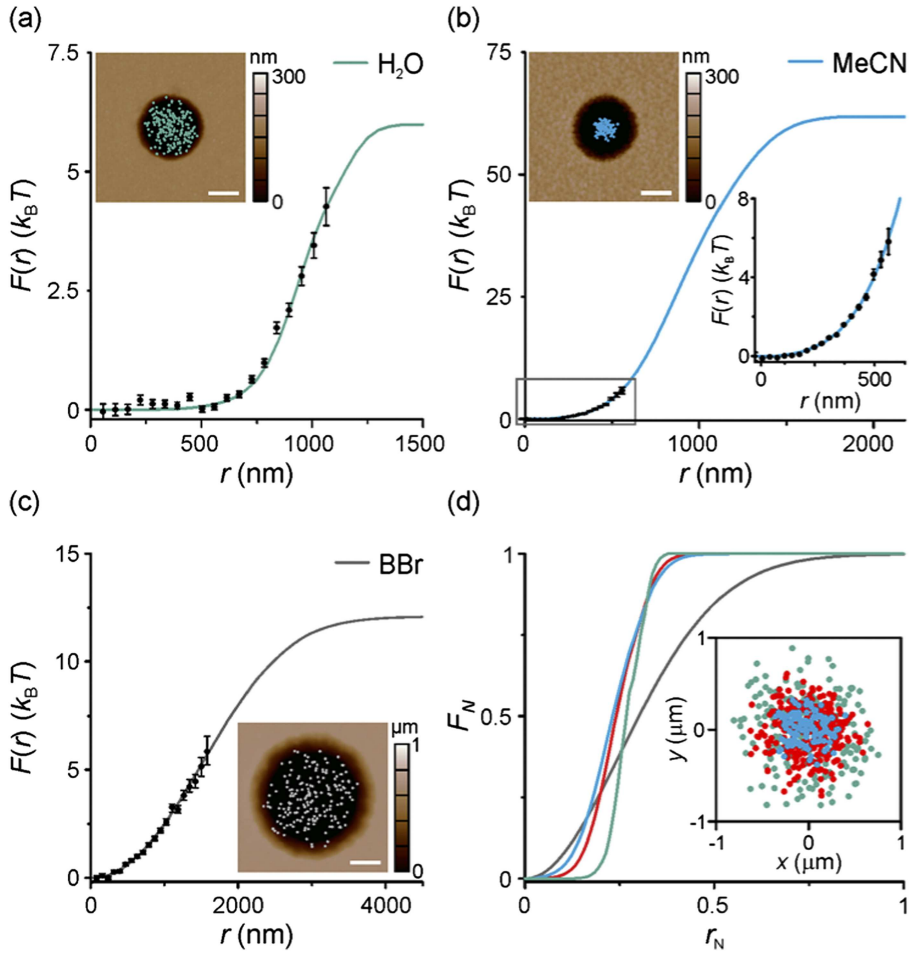

FIG. 3. Experimentally measured (symbols) and calculated (lines) spatial electrostatic free energy profiles, $F(r)$ for a single trapped particle in water (a), acetonitrile (b), and bromobenzene (c). The insets display scatter plots of particle positions overlaid on AFM images of the pockets. Scale bars represent 1 μm. (d) Normalized $F(r)$ values, F_N plotted against the normalized pocket radius, r_N for water (green), acetonitrile (blue), ethanol (red), and bromobenzene (gray). The inset represents spatial scatter plots for single particles in water (green), acetonitrile (blue), and ethanol (red), trapped by the pockets of diameter, D = 2120 ± 80 nm. The plot emphasizes the influence of the Debye length on the degree of confinement of the particle.

as an input parameter to determine σ from the experimentally measured $F(r)$.

A. Comparing experimental measurements with a charge regulation model for the net surface charge of SiO_2

We now compare our experimental measurements with a simple theoretical model for the net surface charge that takes into consideration the dielectric constant, salt concentration, and pH of the solvent. For low surface potentials, the linear regime of the Poisson–Boltzmann equation yields the following relationship between the surface charge and surface potential, $\sigma = \varepsilon_s \kappa \psi_s$. Assuming the surface potential, ψ_s remains constant and we thus expect

$$\sigma \propto \sqrt{\varepsilon_s} \tag{1}$$

at the simplest level of approximation. In practice, however, the relationship between surface charge, surface potential, and system parameters such as κ and ε_s is more accurately described by the following two equations:[32]

TABLE I. Experimentally measured and theoretically estimated parameters for experiments in water (H_2O), acetonitrile (MeCN), ethanol (EtOH), and bromobenzene (BBr). Uncertainties on σ represent standard deviations from 9 to 12 single particle measurements in each solvent, including contributions from uncertainties on particle radius, a and salt concentration, c

		Experimental quantities					Theoretical parameters	
Solvent	ε_s	c, μM	pH	κ^{-1}	p_{fit}	$-\sigma$, 10^{-3} e/nm^2	b	p_{est}
H_2O	78.3	245 ± 9	8.7	19.6 ± 0.3	–	~90	0	-1.2
MeCN	36.64	3.8 ± 0.4	6.1	106 ± 6	3.35	0.8 ± 0.1	1.44	2.84
EtOH	24.3	6.5 ± 0.5	7.3	66 ± 3	3.3	0.9 ± 0.2	2.8	3.0
BBr	5.4	0.040 ± 0.002	-	388 ± 13	1.9	0.35 ± 0.06	17.2	~1.5 to 3.0

$$\psi_s(\sigma) = \frac{k_B T}{e} \ln\left(\frac{-\sigma}{e\Gamma + \sigma}\right) + p\frac{k_B T \ln 10}{e}, \quad (2)$$

$$\sigma(\psi_s) = \frac{2\varepsilon_s \varepsilon_0 \kappa k_B T}{e} \sinh\left(\frac{e\psi_s}{2k_B T}\right), \quad (3)$$

where $p = pK_a - pH$, and we take $\Gamma = 8\ nm^{-2}$ as the density of ionizable surface sites and ignore the Stern layer capacitance.[24] A previous study[33] uses what is essentially a $1 - pK_a$ model for the silica surface, neglects the contribution of the Stern layer, and demonstrates good agreement with potentiometric measurements of surface charge.[34] Note that $\sigma = -e\Gamma_{SiO^-}$ and $\Gamma = \Gamma_{SiO^-} + \Gamma_{SiOH}$.

Equation (2) captures the dependence of the net surface charge, σ on the proton concentration at the surface, which in turn depends on the pH of the bulk electrolyte and the surface potential, ψ_s. Equation (3) is the Grahame equation which comes from integrating the charge density in the diffuse double layer and setting it equal in magnitude to the net surface charge in order to satisfy the requirement of electroneutrality in the system.

The above system of equations contains a single parameter $p = pK_a - pH$, where $pK_{a,w} = 7.5$ denotes the acid dissociation constant of the ionizable surface SiOH groups in water.[24] Although the values of pH and pK_a are readily available for water, they can be difficult to directly measure in apolar media. We therefore treat p as a tunable parameter in applying the model to the solvents EtOH, MeCN, and BBr.

Solving Equations (2) and (3) for various values of p, we note the dependence $\frac{\sigma}{\sqrt{c}} \sim \varepsilon_s^{0.28}$, which is weaker than the square root dependence of (1) (solid line in Fig. 4(a)). However the model also reveals that the surface potential ψ_s itself depends weakly on the solvent dielectric constant as $\psi_s \sim \varepsilon_s^{-0.18}$ (solid line in Fig. 4(b)) which accounts rather well for the net $\sim \varepsilon_s^{0.28}$ dependence of σ at a given salt concentration, c.

Table I lists the measured values of σ and the corresponding best fit values of p, denoted by p_{fit}. We find that the experimental measurements for all the non-aqueous media are captured for $p = 1.9$-3.35 and now proceed to examine the physical relevance of the obtained values.

We begin by estimating $pK_{a,s}$ in each apolar medium starting from the value in water, $pK_{a,w}$. We assume that the electrostatic contribution from the Born solvation energy, b of a proton in a medium of dielectric constant ε_s is the dominant contribution to the shift in acid dissociation constant relative to water, $\Delta pK_{a,s} = pK_{a,s} - pK_{a,w}$.

Thus we have

$$\Delta pK_{a,s} \cong b = \frac{l_{b,w}}{4.606 a_{H^+}}\left(\frac{\varepsilon_w}{\varepsilon_s} - 1\right), \quad (4)$$

where $l_{b,w} = \frac{e^2}{4\pi\varepsilon_w\varepsilon_0 k_B T} = 0.714$ nm is the Bjerrum length in water at 25 °C, $a_{H^+} = 0.122$ nm is the radius of the hydronium ion,[35] and $\varepsilon_w = 78.3$ is the dielectric constant of water. In EtOH, for example, the estimated shift $\Delta pK_{a,s} = 2.8$ implies that the pK_a of the SiOH group would be expected to lie around 10.3. Measurements of the pH of pure ethanol yield a value of 7.3 (see the supplementary material), placing p_{est}, the theoretically estimated value of p at 3.0. This suggests that our experimentally obtained fit value, $p_{fit} = 3.3$ is indeed plausible.

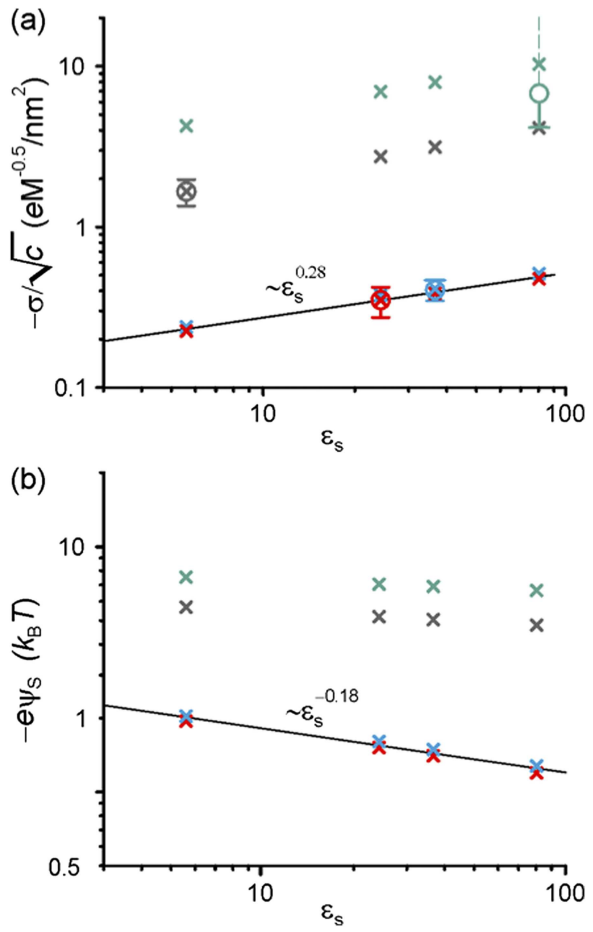

FIG. 4. (a) Theoretical dependence of $\frac{\sigma}{\sqrt{c}}$ on the solvent dielectric constant, ε_s calculated from the charge regulation model given by Equations (2) and (3) (colored crosses). Colors denote calculations of $\frac{\sigma}{\sqrt{c}}$ performed over the entire range of ε_s using specific combinations of the salt concentration, c and the corresponding best-fit p value (see Table I) for the relevant experimental measurement. Experimental measurements are denoted by open circular symbols at the relevant value of ε_s. The solid line represents $\frac{\sigma}{\sqrt{c}} \sim \varepsilon_s^{0.28}$ dependence. (b) Theoretical dependence of the SiO_2 surface potential, ψ_s on ε_s corresponding to the calculations in (a). Solid line denotes $\psi_s \sim \varepsilon_s^{-0.18}$ dependence.

Similarly for acetonitrile, taking the experimentally inferred background conductivity of 0.3 μM of monovalent ions as an order of magnitude estimate of the free proton concentration points to $pH_{MeCN} = 6.5$, which is in fact reasonably close to our measured value of $pH_{MeCN} = 6.1$ (the supplementary material). $\Delta pK_{a,s} = 1.44$ estimated using Eq. (4) and $pH_{MeCN} = 6.1$ together imply an independently determined value of $p_{est} = 2.84$, which again compares reasonably well with the experimentally obtained $p_{fit} = 3.35$.

In BBr, the background solvent conductivity is too small to be directly measured (<0.005 μS/cm) and so we cannot estimate the pH independently. However we note that the measured pH of EtOH and MeCN roughly points to the relation pH_s-$pH_w \sim b$. Here the effective pH of pure water, pH_w is around 5.5-6 owing to the dissolution of CO_2 from the atmosphere[36] and pH_s is the pH of the solvent under consideration. Since it may be reasonable to assume that pH_s and the acid dissociation constant $pK_{a,s}$ of the surface ionizable groups in the solvent respond to a first approximation in a similar way

TABLE II. Comparison of our measured surface charge, σ with that obtained from electrophoretic mobility measurements. ζ—measured zeta potential; σ_{zeta}—the corresponding surface charge density; ψ_s—surface potential corresponding to σ

Solvent	$-\zeta$, (mV)	$-\sigma_{zeta}$, $10^{-3}e/nm^2$	$-\psi_s$, mV	$-\sigma$, $10^{-3}e/nm^2$
H_2O	71 ± 15	22 ± 7 (23 ± 8)	140	~90
MeCN	36 ± 27	0.7 ± 0.6 (1.0 ± 0.9)	38 ± 4	0.8 ± 0.1
EtOH	44 ± 13	1.0 ± 0.4 (1.2 ± 0.4)	39 ± 6	0.9 ± 0.2

to ε_s, taking water ($p \sim 2$) as the reference state, the measurement for BBr might also be expected to be captured by a value of $p \sim 1.5$ to 3. In fact we find good agreement between the measured net charge density of SiO_2 and the value predicted by the charge regulation model for p = 1.9.

Finally, for experiments in water at pH 8.7, we find that the experimentally estimated σ is in order of magnitude agreement with the model prediction for p = −1.2. Overall our study shows that the pK_a of the ionizable groups and pH of the solvent phase play a strong role in determining the net electrical charge of an ionizable surface in media of various polarities. Interestingly we find that although BBr has a dielectric constant ≃7 times smaller than that of MeCN, at -0.35×10^{-3} e/nm^2 the net charge density of SiO_2 in BBr is smaller than that in MeCN by not much more than a factor of 2. The same value is however around an order of magnitude smaller than the measured surface charge of mica in contact with nonpolar solvents containing surfactants.[6]

To conclude, Table II presents measured zeta potentials, ζ, for silica microspheres, and surface charge density values, σ_{zeta} calculated using Equation (3), where $\psi_s = \zeta$. The values in parentheses include the curvature correction due to finite κa.[24] Comparing these values with those obtained using our approach, it is interesting to note that in the linear regime, $e|\psi_s| \sim k_BT$ ($|\psi_s| \sim 25$ mV), which holds for EtOH and MeCN, both methods agree well. But in water where surfaces are strongly charged and non-linearities become important, our approach is able to capture the theoretical prediction, where the corresponding mobility-based value significantly underestimates both surface charge and surface potential.

IV. CONCLUSION

We have demonstrated the use of an electrostatic fluidic trap to directly measure the net surface charge density of ionizable surfaces over a wide range of solvent polarity. The experimental approach is highly versatile, can be applied to solvents of any polarity and composition, makes use of any optically detectable probe particle, and does not involve the use of external electric fields. We find that the measurements can be captured by a charge regulation model containing a single tunable parameter whose value was found physically plausible in all cases. The charge regulation model we tested captures our measurements over a wide range of polarities tested and may find general applicability in estimating the magnitude of net surface charge and electrostatic interactions in experiments in apolar media. Furthermore our technique may be thought of as a form of optical force microscopy with the crucial advantage that it replaces the relatively challenging measurement of a highly calibration-sensitive axial particle-surface interaction potential[37] with a direct measurement based on calibration-free, in-plane spatial information on particle position. Probing an equilibrium interaction at the single particle level, the method also successfully sidesteps concerns on pair-wise additivity of interparticle potentials that often arise in measurements of long-ranged interactions in particle ensembles.

SUPPLEMENTARY MATERIAL

See supplementary material for conductivity-concentration calibration curves, SiO_2 microsphere size distribution measurements, and pH measurements for EtOH and MeCN.

ACKNOWLEDGMENTS

We gratefully acknowledge the Swiss National Science Foundation and University of Zurich for financial support. Nanofabrication was carried out at FIRST Center for Micro- and Nanoscience, ETH Zurich.

[1] E. Verwey and J. T. G. Overbeek, *Theory of the Stability of Lyophobic Colloids* (Elsevier Publishing Company, 1948).
[2] G. S. Roberts, T. A. Wood, W. J. Frith, and P. Bartlett, "Direct measurement of the effective charge in nonpolar suspensions by optical tracking of single particles," J. Chem. Phys. **126**, 194503 (2007).
[3] S. K. Sainis, V. Germain, C. O. Mejean, and E. R. Dufresne, "Electrostatic interactions of colloidal particles in nonpolar solvents: Role of surface chemistry and charge control agents," Langmuir **24**, 1160–1164 (2008).
[4] P. G. Smith, M. N. Patel, J. Kim, T. E. Milner, and K. P. Johnston, "Effect of surface hydrophilicity on charging mechanism of colloids in low-permittivity solvents," J. Phys. Chem. C **111**, 840–848 (2007).
[5] C. E. McNamee, Y. Tsujii, and M. Matsumoto, "Interaction forces between two silica surfaces in an apolar solvent containing an anionic surfactant," Langmuir **20**, 1791–1798 (2004).
[6] W. H. Briscoe and R. G. Horn, "Direct measurement of surface forces due to charging of solids immersed in a nonpolar liquid," Langmuir **18**, 3945–3956 (2002).
[7] F. Strubbe, F. Beunis, and K. Neyts, "Determination of the effective charge of individual colloidal particles," J. Colloid Interface Sci. **301**, 302–309 (2006).
[8] J. N. Munday, F. Capasso, and V. A. Parsegian, "Measured long-range repulsive Casimir-Lifshitz forces," Nature **457**, 170–173 (2009).
[9] J. Ge, L. He, J. Goebl, and Y. Yin, "Assembly of magnetically tunable photonic crystals in nonpolar solvents," J. Am. Chem. Soc. **131**, 3484–3486 (2009).
[10] M. E. Leunissen, C. G. Christova, A.-P. Hynninen, C. P. Royall, A. I. Campbell, A. Imhof, M. Dijkstra, R. Van Roij, and A. Van Blaaderen, "Ionic colloidal crystals of oppositely charged particles," Nature **437**, 235–240 (2005).
[11] P. Bartlett and A. I. Campbell, "Three-dimensional binary superlattices of oppositely charged colloids," Phys. Rev. Lett. **95**, 128302 (2005).
[12] R. J. Pugh, T. Matsunaga, and F. M. Fowkes, "The dispersibility and stability of carbon-black in media of low dielectric-constant. 1. Electrostatic and steric contributions to colloidal stability," Colloids Surf. **7**, 183–207 (1983).
[13] B. Comiskey, J. Albert, H. Yoshizawa, and J. Jacobson, "An electrophoretic ink for all-printed reflective electronic displays," Nature **394**, 253–255 (1998).
[14] Y. Chen, J. Au, P. Kazlas, A. Ritenour, H. Gates, and M. McCreary, "Electronic paper: Flexible active-matrix electronic ink display," Nature **423**, 136 (2003).
[15] R. Kornbrekke, I. Morrison, and T. Oja, "Electrophoretic mobility measurements in low conductivity media," Langmuir **8**, 1211–1217 (1992).
[16] J. F. Miller, K. Schtzel, and B. Vincent, "The determination of very small electrophoretic mobilities in polar and nonpolar colloidal dispersions using phase analysis light scattering," J. Colloid Interface Sci. **143**, 532–554 (1991).

[17]F. Beunis, F. Strubbe, K. Neyts, and D. Petrov, "Beyond Millikan: The dynamics of charging events on individual colloidal particles," Phys. Rev. Lett. **108**, 016101(2012).
[18]A. T. Prez and E. Lemaire, "Measuring the electrophoretic mobility of concentrated suspensions in nonaqueous media," J. Colloid Interface Sci. **279**, 259–265 (2004).
[19]M. F. Hsu, E. R. Dufresne, and D. A. Weitz, "Charge stabilization in nonpolar solvents," Langmuir **21**, 4881–4887 (2005).
[20]M. Krishnan, N. Mojarad, P. Kukura, and V. Sandoghdar, "Geometry-induced electrostatic trapping of nanometric objects in a fluid," Nature **467**, 692–695 (2010).
[21]N. Mojarad and M. Krishnan, "Measuring the size and charge of single nanoscale objects in solution using an electrostatic fluidic trap," Nat. Nanotechnol. **7**, 448–452 (2012).
[22]M. Krishnan, "Electrostatic free energy for a confined nanoscale object in a fluid," J. Chem. Phys. **138**, 114906 (2013).
[23]N. Mojarad, V. Sandoghdar, and M. Krishnan, "Measuring three-dimensional interaction potentials using optical interference," Opt. Express **21**, 9377–9389 (2013).
[24]S. H. Behrens and D. G. Grier, "The charge of glass and silica surfaces," J. Chem. Phys. **115**, 6716–6721 (2001).
[25]R. J. LeSuer, C. Buttolph, and W. E. Geiger, "Comparison of the conductivity properties of the tetrabutylammonium salt of tetrakis(pentafluorophenyl)borate anion with those of traditional supporting electrolyte anions in nonaqueous solvents," Anal. Chem. **76**, 6395–6401 (2004).
[26]W. P. Wong and K. Halvorsen, "The effect of integration time on fluctuation measurements: Calibrating an optical trap in the presence of motion blur," Opt. Express **14**, 12517–12531 (2006).
[27]W. P. Wong and K. Halvorsen, "Beyond the frame rate: Measuring high-frequency fluctuations with light-intensity modulation," Opt. Lett. **34**, 277–279 (2009).
[28]J. T. G. Overbeek, "The role of energy and entropy in the electrical double-layer," Colloids Surf. **51**, 61–75 (1990).
[29]M. E. Leunissen, J. Zwanikken, R. Van Roij, P. M. Chaikin, and A. Van Blaaderen, "Ion partitioning at the oilwater interface as a source of tunable electrostatic effects in emulsions with colloids," Phys. Chem. Chem. Phys. **9**, 6405–6414 (2007).
[30]C. P. Royall, M. E. Leunissen, and A. van Blaaderen, "A new colloidal model system to study long-range interactions quantitatively in real space," J. Phys.: Condens. Matter **15**, S3581–S3596 (2003).
[31]J. Zwanikken and R. Van Roij, "Inflation of the screening length induced by Bjerrum pairs," J. Phys.: Condens. Matter **21**, 424102 (2009).
[32]T. Hiemstra, W. H. Riemsdijk, and G. H. van and Bolt, "Multisite proton adsorption modeling at the solid/solution interface of (hydr) oxides: A new approach," J. Colloid Interface Sci. **133**, 91–104(1989).
[33]M. Barisik, S. Atalay, A. Beskok, and S. Qian, "Size dependent surface charge properties of silica nanoparticles," J. Phys. Chem. C **118**, 1836–1842 (2014).
[34]M. Kobayashi, F. Juillerat, P. Galletto, and M. Borkovec, "Aggregation and charging of colloidal silica particles: Effect of particle size," Langmuir **21**, 5761–5769 (2005).
[35]J. T. Rubino and W. S. Berryhill, "Effects of solvent polarity on the acid dissociation-constants of benzoic-acids," J. Pharm. Sci. **75**, 182–186 (1986).
[36]J. D. Hem, *Study and Interpretation of the Chemical Characteristics of Natural Water* (U.S. Geological Survey, 1985).
[37]D. C. Prieve, "Measurement of colloidal forces with tirm," Adv. Colloid Interface Sci. **82**, 93–125 (1999).